BiSbTe-Based Nanocomposites with High *ZT*: The Effect of SiC Nanodispersion on Thermoelectric Properties

Jianhui Li, Qing Tan, Jing-Feng Li, Da-Wei Liu, Fu Li, Zong-Yue Li, Minmin Zou, and Ke Wang*

Thermoelectric materials have potential applications in energy harvesting and electronic cooling devices, and bismuth antimony telluride (BiSbTe) alloys are the state-of-the-art thermoelectric materials that have been widely used for several decades. It is demonstrated that mixing SiC nanoparticles into the BiSbTe matrix effectively enhances its thermoelectric properties; a high dimensionless figure of merit (*ZT*) value of up to 1.33 at 373 K is obtained in $Bi_{0.3}Sb_{1.7}Te_3$ incorporated with only 0.4 vol% SiC nanoparticles. SiC nano-inclusions possessing coherent interfaces with the $Bi_{0.3}Sb_{1.7}Te_3$ matrix can increase the Seebeck coefficient while increasing the electrical conductivity, in addition to its effect of reducing lattice thermal conductivity by enhancing phonon scattering. Nano-SiC dispersion further endows the BiSbTe alloys with better mechanical properties, which are favorable for practical applications and device fabrication.

1. Introduction

Thermoelectric materials have attracted increasing attention recently because of its important applications of energy harvesting and electronic cooling devices.[1–4] Generally, the efficiency of a thermoelectric device is closely related to the materials' dimensionless figure of merit, defined as $ZT = \alpha^2\sigma T/\kappa$, where α, σ, κ and T are the Seebeck coefficient, electrical conductivity, thermal conductivity and absolute temperature, respectively.[3,4] It is clear that a high-*ZT* material must possess a high Seebeck coefficient, high electrical conductivity and low thermal conductivity. However, these parameters are closely interrelated because they are determined by more fundamental characteristics of the electron and phonon systems.[4,5] Increasing electrical conductivity usually results in a decrease of the Seebeck coefficient. Similarly, the reduction of thermal conductivity often leads to a decrease in electrical conductivity. Fortunately, several successful examples have been reported in the past decade, in which *ZT* enhancement is realized by decoupling the electrical and thermal transport properties even in bulk materials. The main approach is to incorporate nanoscale heterogeneity or nanoinclusions into a thermoelectric alloy matrix mainly by in situ precipitation or reaction.[6–10] For example, enhanced thermoelectric properties have been achieved in the $AgPb_mSbTe_{m+2}$ system with characteristic nanostructures of nanoscale inhomogeneity (rich in Ag and Sb) embedded in the PbTe matrix;[6,7] in fact, $AgPb_mSbTe_{m+2}$ can be considered to be antimony and silver co-doped PbTe. It has been revealed that nanoscopic inhomogeneity effectively reduces thermal conductivity of the whole material by enhancing phonon scattering but show less influences on its electrical conductivity because of their coherent interfaces formed through in situ precipitation. Zhao et al.[10] fabricated a nanostructured composite containing ytterbium-filled $CoSb_3$ and well-distributed Yb_2O_3 particles synthesized by in situ oxidation. The Yb_2O_3 nanoparticles dispersed both at grain boundaries and inside grains generate a combined effect that considerably scatters phonons but only slightly impacts electrons, thereby providing a significant *ZT* enhancement.

In general, it seems also possible to enhance *ZT* values by dispersing nanoparticles in a thermoelectric material using a mixing method, but it is difficult to find such a material combination that thermal conductivity is reduced while its electrical conductivity is not reduced significantly at the same time by incorporating nanoparticles. Nevertheless, adding SiC nanoparticles into Bi_2Te_3-based alloys is a good choice, in view of the facts that SiC is a promising thermoelectric semiconductor with a wide bandgap and large Seebeck coefficient as well as relatively high electrical conductivity.[11] In addition, the introduction of hard SiC nanoparticles can improve the mechanical property of thermoelectric materials and hence benefit device fabrication.[12–14]

This work demonstrates that mixing SiC nanoparticles into the p-type BiSbTe matrix is effective for its thermoelectric property enhancement; a high *ZT* value up to 1.33 at 373 K was obtained in $Bi_{0.3}Sb_{1.7}Te_3$ alloys by incorporating an optimized amount of nano-SiC particles. The nanostructure including the interfaces between SiC and the matrix was investigated to explore the mechanism why thermoelectric performance can be enhanced in a nanoparticle-dispersed composite fabricated by a mixing method.

Dr. J. H. Li, Q. Tan, Prof. J.-F. Li, D.-W. Liu, F. Li, Z.-Y. Li, M. M. Zou, Dr. K. Wang
State Key Laboratory of New Ceramics and Fine Processing
School of Materials Science and Engineering
Tsinghua University
Beijing, 100084, China
E-mail: jingfeng@mail.tsinghua.edu.cn

DOI: 10.1002/adfm.201300146

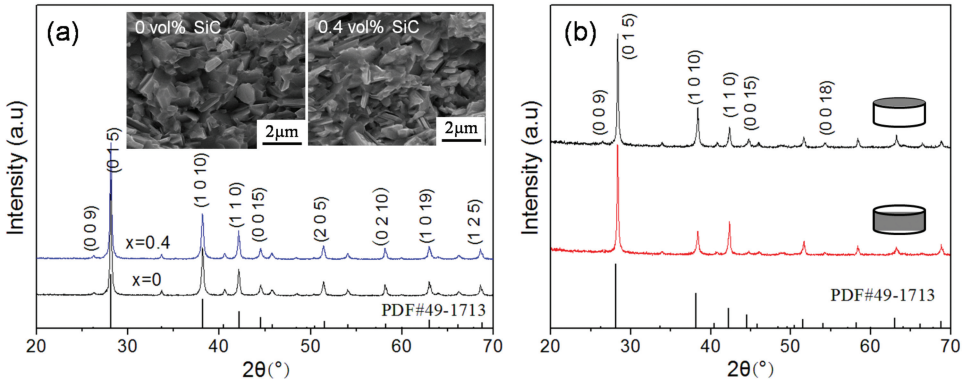

Figure 1. a) XRD patterns and SEM microstructures for fractured surface of $Bi_{0.3}Sb_{1.7}Te_3$+ *x* vol% SiC (*x* = 0, 0.4) sintered by SPS at 673 K. b) XRD patterns of the sample sections perpendicular and parallel to the pressing direction $Bi_{0.3}Sb_{1.7}Te_3$+0.4 vol% SiC.

2. Results and Discussion

Figure 1a shows the XRD patterns of two representative samples with/without SiC addition; the diffraction peaks cited from the database of the $Bi_{0.5}Sb_{1.5}Te_3$ (PDF#49-1713) are also given in the bottom of the figure by the vertical lines. All the diffraction patterns of the two samples match well with the standard peaks of $Bi_{0.5}Sb_{1.5}Te_3$. No diffraction peaks of SiC are detected in the $Bi_{0.3}Sb_{1.7}Te_3$ + 0.4 vol% SiC sample owing to its low content, but its existence was confirmed by EPMA and TEM as shown later. In addition, by taking the sample with 0.4 vol%SiC for an example, the XRD patterns of the sample sections perpendicular and parallel to the pressing direction are given in Figure 1b and the orientation factor F was also calculated using the following equations.[15]

$$F = \frac{P - P_0}{1 - P_0} \quad (1)$$

$$P_0 = \frac{I_0(00l)}{\sum I_0(hkl)} \quad (2)$$

$$P = \frac{I(00l)}{\sum I(hkl)} \quad (3)$$

where P and P_0 are the integrated intensities of all (00*l*) planes to the intensities of all (*hkl*) planes for preferentially and randomly oriented samples. It can be found that the relative intensities of (00*l*) planes from the sections perpendicular to the pressing direction are slightly higher than those from the sections parallel to the pressing direction. However, the orientation degree of the planes, termed F was 0.07, which means that no preferential orientation formed in the present samples although it was reported[16] in some Bi_2Te_3-based materials fabricated by pressurized sintering such as SPS, probably because the MA-derived particles are considerably fine and their preferential grain growth is suppressed when sintered at the low temperature and within a short time. As shown in the insert of Figure 1a, relatively fine grains are obtained both in the sample with/without SiC addition, since the MA-SPS method has an advantage of producing fine-grained materials; MA-derived fine powders can be densified at reduced temperatures and in a short period by SPS. Moreover, the grain size of the composite with 0.4 vol% SiC decreases somewhat as compared with that of $Bi_{0.3}Sb_{1.7}Te_3$, which suggests that the dispersion of nano-SiC particles suppresses the grain growth of the matrix materials. As shown in the scanning electron microscopy (SEM) images, a lot of plate-shaped grains can be observed, which are characteristics of the layer structure of Bi_2Te_3-based compounds.

Electronic probe micro-analyzer (EPMA) and transmission electron microscopy (TEM) experiments were conducted to confirm the existence of SiC phase. As shown in **Figure 2**, the Si element was detected in spite of its weak signal with some Si-rich areas corresponding to the SiC nanoparticles. The EPMA experiments also confirmed that SiC nanoparticles are homogeneously distributed throughout the sample although its volume fraction is as low as 0.4%. **Figure 3** shows the TEM and high-resolution TEM (HRTEM) images of $Bi_{0.3}Sb_{1.7}Te_3$ dispersed with nano-SiC particles. Figure 3a shows an HRTEM image of $Bi_{0.3}Sb_{1.7}Te_3$ matrix, in which we can find many lattice stripes with definite widths, and Figure 3b is an amplified HRTEM image of the white rectangle area in Figure 3a. A series of two rows of extra-bright dots are separated by four weaker bright dot rows, forming five-layer lamellae. Lan et al.[17] investigated the structure of nanograined $Bi_xSb_{2-x}Te_3$ bulk materials prepared by a ball milling and hot-pressing method, and observed both five-layer lamellae and seven-layer lamellae. In this work, only five-layer lamellae are found, and such five-layer lamellae are also found in the sample without nano-SiC. It is likely that five-layer lamellae represent the ideal structure of Bi_2Te_3,[17] which implies that more ideal structure might be formed in the $Bi_{0.3}Sb_{1.7}Te_3$ composite prepared by MA-SPS method. As shown in Figure 3c, some SiC particles with diameters ranging from several tens to one hundred nanometers are observed both at grain boundaries and inside grains in the SiC-dispersed sample. We conducted a lot of observations by focusing on the interface between the $Bi_{0.3}Sb_{1.7}Te_3$ matrix and the nano-SiC particles, and one typical HRTEM image is shown in Figure 3d. Surprisingly, the interfaces are found to be quite "clean" and even coherent in most places. Considering that the lattice constants of cubic SiC (a = 0.436 nm) are close to that of $Bi_{0.3}Sb_{1.7}Te_3$, which has a hexagonal unit cell with lattice

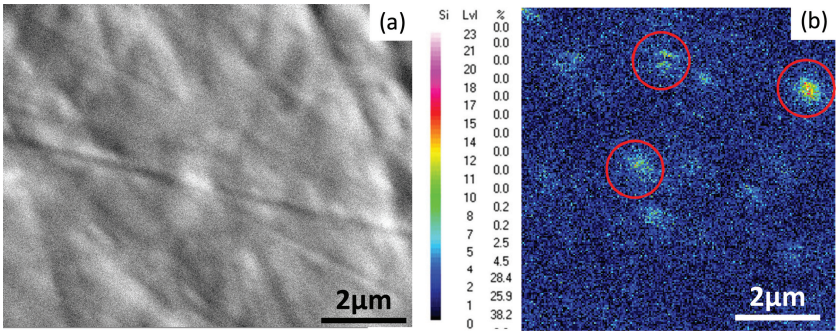

Figure 2. a) SEM secondary electron images of a polished surface of $Bi_{0.3}Sb_{1.7}Te_3$ + 0.4 vol% SiC and b) X-ray map of Si. SiC nanoparticles are located at the circled areas with high Si concentration.

constants $a = 0.429$ nm and $c = 3.048$ nm, it is possible to form coherent interfaces between SiC and $Bi_{0.3}Sb_{1.7}Te_3$. It should be mentioned that $Bi_{0.3}Sb_{1.7}Te_3$ was formed by mechanical alloying of Bi, Sb and Te elemental powders with the presence of SiC nanoparticles, which may act as the nucleation site for the mechanochemical formation of $Bi_{0.3}Sb_{1.7}Te_3$. Therefore, the present fabrication process is also in favor for the formation of coherently bonded interfaces. For Figure 3d, additional analysis was done to confirm the interface between $Bi_{0.3}Sb_{1.7}Te_3$ and SiC. Here, the Fourier transfer diffraction pattern of Figure 3d is given in Figure 3e, and that of $Bi_{0.3}Sb_{1.7}Te_3$ matrix for comparison is also given in Figure 3f. We can find that there are some extra diffraction spots in Figure 3e as compared with 3f, as pointed out by the red circles that belong to SiC, indicating the existence of SiC in addition to the $Bi_{0.3}Sb_{1.7}Te_3$ matrix.

Figure 4 shows the temperature dependence of electrical conductivity, Seebeck coefficient and power factor for $Bi_{0.3}Sb_{1.7}Te_3$+ x vol% SiC ($x = 0$, 0.1, 0.4, 0.6), and the ratio of Seebeck coefficient to electrical resistivity of $Bi_{0.3}Sb_{1.7}Te_3$ with different contents of nano-SiC at 323 and 423 K is also given. As shown in Figure 4a, the electrical conductivity of all samples decreases with temperature, being indicative of semimetallic transport behavior. The tiny amount of SiC addition did not cause significant change in electrical conductivity. Nevertheless, it seems that the highest electrical conductivity value (10.2×10^4 S m^{-1}) was obtained in the $Bi_{0.3}Sb_{1.7}Te_3$ + 0.4 vol% SiC sample, implying that the electrical conductivity can be increased by incorporating an optimized small amount of SiC particles into $Bi_{0.3}Sb_{1.7}Te_3$, although the former has lower electrical conductivity. As shown in **Table 1**, the carrier concentration is increased from 1.81×10^{19} cm^{-3} for $Bi_{0.3}Sb_{1.7}Te_3$ to 3.39×10^{19} cm^{-3} for the sample with 0.4 vol% SiC, although the carrier mobility is correspondingly reduced from 365.4 cm^2 V^{-1} s^{-1} to 212.1 cm^2 V^{-1} s^{-1}. The SiC addition reduces the grain size and increases the defects, which can increase the carrier density, and decrease the mobility by enhancing scattering. Therefore, the SiC addition can increase the electrical conductivity of $Bi_{0.3}Sb_{1.7}Te_3$ provided that the carrier concentration is sufficiently increased to compensate for the reduction of carrier mobility. It should be mentioned that the coherent interfaces between $Bi_{0.3}Sb_{1.7}Te_3$ and nano-SiC could weaken the obstructing effect of nanoinclusions against carrier transport,[7,18] consequently the carrier mobility is still high even in the SiC-dispersed $Bi_{0.3}Sb_{1.7}Te_3$.

Figure 4b shows the temperature dependence of Seebeck coefficient for $Bi_{0.3}Sb_{1.7}Te_3$ + x vol% SiC ($x = 0$, 0.1, 0.4, 0.6) compositions. The Seebeck coefficient values for all samples are positive, indicative of p-type electrical transport property. It has also been revealed[19] that nano-SiC dispersion is effective in improving the thermoelectric properties of p-type $Bi_{0.5}Sb_{1.5}Te_3$ compound rather than n-type $Bi_2Te_{2.7}Se_{0.3}$, probably because of p-type semiconducting characteristic of SiC.[11] The Seebeck coefficient values for all samples increase with temperature approximately below 423 K and then turn to decrease. It reaches a maximum value of 211 μV K^{-1} around 427 K when the nano-SiC content is 0.4 vol%, which is somewhat higher than that of $Bi_{0.3}Sb_{1.7}Te_3$ (206 μV K^{-1} at 427 K). Interestingly, the Seebeck coefficient value increases although the electrical conductivity increases by

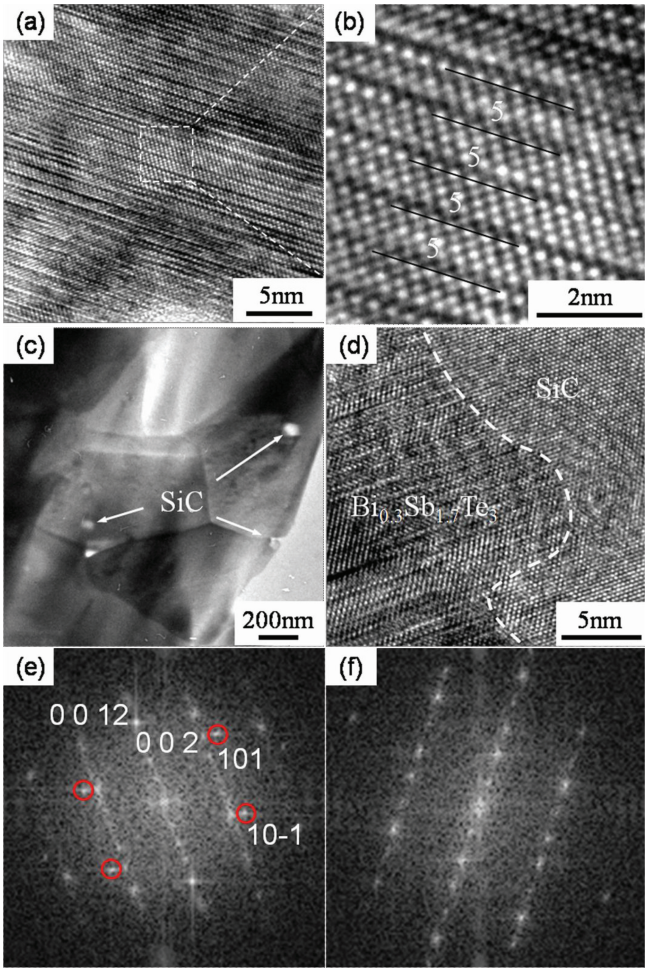

Figure 3. TEM and HRTEM images of the sample dispersed with nano-SiC: a) HRTEM image of $Bi_{0.3}Sb_{1.7}Te_3$ matrix; b) high-magnification image of the white rectangle area in (a); c) TEM image of nano-SiC in $Bi_{0.3}Sb_{1.7}Te_3$ matrix; d) HRTEM image of the interface between $Bi_{0.3}Sb_{1.7}Te_3$ matrix and nano-SiC; and e,f) the Fourier transfer diffraction pattern of (d) and (a), respectively.

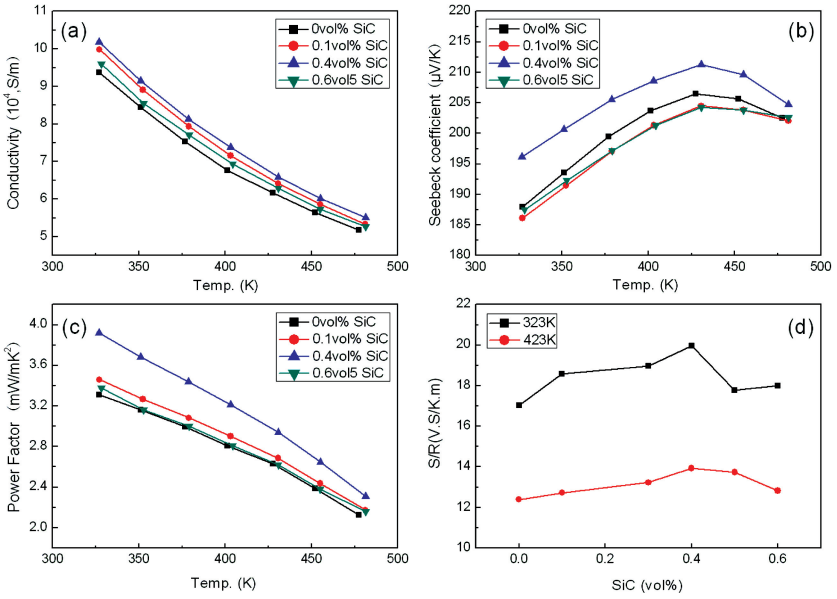

Figure 4. Temperature dependence of a) electrical conductivity, b) Seebeck coefficient, c) power factor for $Bi_{0.3}Sb_{1.7}Te_3$ + *x* vol% SiC (*x* = 0, 0.1, 0.4, 0.6) samples, and d) the ratio of Seebeck coefficient to electrical resistivity at 323 and 423 K of $Bi_{0.3}Sb_{1.7}Te_3$ + *x* vol% SiC (*x* = 0, 0.1, 0.3, 0.4, 0.5, 0.6) compositions as a function of the volume fraction of nano-SiC.

adding SiC nanoparticles into $Bi_{0.3}Sb_{1.7}Te_3$, although it is generally known that absolute Seebeck coefficient decreases if the electrical conductivity improves. With the values of electrical conductivity and Seebeck coefficient mentioned above, the power factor values of all samples are calculated and the results are shown in Figure 4c. The power factor values increase with the addition of nano-SiC, and reaches a maximum when the addition is 0.4 vol% with a high value of 3.92 mW K^{-2} m^{-1} around 327 K, but turns to decrease to a value close to that of $Bi_{0.3}Sb_{1.7}Te_3$ without SiC addition if the SiC addition is further increased. Figure 4d shows the change in the ratio of Seebeck coefficient to electrical resistivity at 323 and 423 K as a function of the volume fraction of nano-SiC. With increasing the content of nano-SiC, the ratio increases gradually and gets the maximum when the SiC addition is 0.4 vol%, then turns to decrease at a higher SiC content, especially at 323 K, clearly indicating that the Seebeck coefficient is enhanced relative to the electrical resistivity.

Generally, the Seebeck coefficient α and electrical conductivity σ are given in Equation (4) and Equation (5):[5,20]

Table 1. Seebeck coefficient, carrier concentration and mobility of all samples at 323 K, and the ratio of effective mass (m^*) between the sample with/without nano-SiC is also listed.

Sample	Seebeck coefficient [μV K^{-1}]	Carrier concentration [10^{19} cm^{-3}]	Carrier mobility [cm^2 V^{-1} s^{-1}]	m_x^*/m_0^*
x = 0	187.94	1.81	365.4	1
x = 0.1	186.14	2.48	284.2	1.222
x = 0.4	196.18	3.39	212.1	1.586
x = 0.6	187.52	3.51	164.1	1.552

$$\alpha = \frac{8\pi^2 k_B^2}{3eh^2} m^* T\left(\frac{\pi}{3n}\right)^{2/3} \quad (4)$$

$$\sigma = 1/\rho = ne\mu \quad (5)$$

where k_B, e, h, m^*, n and μ are Boltzmann constant, electronic charge, Planck constant, effective mass of carrier, carrier concentration and carrier mobility, respectively. Accordingly, the electrical conductivity increases with carrier concentration, but the Seebeck coefficient decreases. However, a different trend was observed in this work. So, what kind of role does nano-SiC act in the composite? Nanoinclusions in a thermoelectric matrix can perform as energy filters,[3,21–24] implying that the increased Seebeck coefficient in the present nanocomposites may be due to the energy filtering effect of nano-SiC. Coherent interfaces can be formed in the combination of $Bi_{0.3}Sb_{1.7}Te_3$ and SiC, which is also prerequisite to the energy filtering effect. In a review paper,[3] Dresselhaus et al. summarized many studies and concluded that nanoparticle inclusions through a size-dependent energy-filtering effect can significantly enhance Seebeck coefficient. The low-energy electrons that contribute less to the electrical conductivity can be strongly scattered, and the Seebeck coefficient depends on the energy derivative of the relaxation time at the Fermi energy, so this type of energy filtering is precisely the prescription to increase the Seebeck coefficient of thermoelectric materials.[24] Xiong et al.[22] indicates that the optimized addition has a close relationship with the size of nanoinclusions. As schematically shown in **Figure 5**, if viewed in three dimensions, the carriers have many possibilities to collide against SiC nanoparticles embedded in the $Bi_{0.3}Sb_{1.7}Te_3$ polycrystalline matrix, even though their volume fraction is extremely low provided that their distribution are spatially homogeneous. The SiC nanoparticles in a series of planes normal to the temperature gradient can filter out many low-energy carriers by the scattering effect, consequently high-energy carriers pass through the SiC nanoinclusions and the material's Seebeck coefficient is enhanced. As another possible reason, the increased Seebeck coefficient may be as a result of the enhanced density of states (DOS) $g(E)$ in the composites.[25,26] As shown in Equation (6),[26] there is a proportional relationship between DOS and effective mass (m^*), and the effective mass (m_x^*) in the nanocomposites can be estimated by calculating its relative value referring to the effective mass (m_0^*) without SiC addition by Equation (7), which can be deduced from Equation (4).

$$g(E) = \frac{(m^*)^{2/3}\sqrt{2E}}{h^3\pi^2} \quad (6)$$

$$\frac{m_x^*}{m_0^*} = \frac{a_x}{a_0}\left(\frac{n_x}{n_0}\right)^{2/3} \quad (7)$$

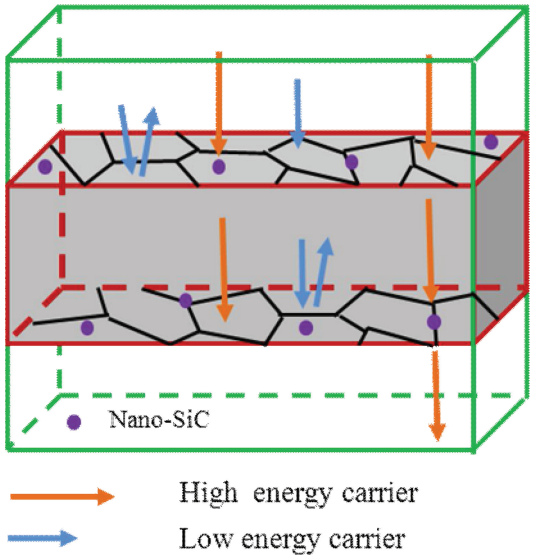

Figure 5. Schematic drawing shows that SiC nanoparticles in a series of planes can block low-energy carriers by energy filtering effect. A low-energy carrier passing though the upper plane can be scattered by SiC nanoparticles at another plane.

According to α and n values measured, the values of m_x^*/m_0^* at 323 K were obtained and shown in Table 1. The m_x^*/m_0^* ratio increased with the addition of nano-SiC, showing a maximum when the addition of SiC is 0.4 vol%, which is consistent with Seebeck coefficient. In the present study, the increase of DOS can be attributed to the change of electronic structures of $Bi_{0.3}Sb_{1.7}Te_3$ due to addition of nano-SiC. The HRTEM results show that, in the nanocomposite, SiC nanoparticles are distributed in grains or along grain boundaries with coherent interfaces with the $Bi_{0.3}Sb_{1.7}Te_3$ matrix, which is required for nanoinclusions to be able to influence the distribution of energy levels of the host material at the interfaces.

Since the highest power factor was obtained at $Bi_{0.3}Sb_{1.7}Te_3$ + 0.4 vol% SiC, its thermal properties were thoroughly investigated and compared with that of $Bi_{0.3}Sb_{1.7}Te_3$. The thermal diffusivity was measured by the laser flash technique in the temperature range from 300 to 500 K and the results are shown in **Figure 6**a. The thermal diffusivity values of two samples decrease with temperature but turn to increase after a minimum at 423 K. It should be noted that their values are close to each other in the whole temperature range. The sintered density values of $Bi_{0.3}Sb_{1.7}Te_3$ and $Bi_{0.3}Sb_{1.7}Te_3$ + 0.4 vol% SiC are 6.649 g cm^{-3} and 6.604 g cm^{-3}, respectively, corresponding to relative densities of 99.7% and 96.2%; the theoretical density values of $Bi_{0.5}Sb_{1.5}Te_3$ and SiC are 6.878 g cm^{-3} and 3.215 g cm^{-3}, respectively. The specific heat values of the present $Bi_{0.3}Sb_{1.7}Te_3$ and $Bi_{0.3}Sb_{1.7}Te_3$ + 0.4 vol% SiC samples were measured using a differential scanning calorimeter (DSC) and the laser flash method, and the results are close to each other. The results shown in Figure 6b are the average values. The measured C_p value is 0.184 J g^{-1} K^{-1} at 373 K, which is very close to that of p-type $Bi_{0.52}Sb_{1.48}Te_3$ at room temperature reported by Xie et al.[27] as shown in Figure 6b; the limited difference may be due to the inconsistent Bi/Sb ratios. Because SiC has a higher C_p, whose room-temperature value is between 0.711 J/g K for cubic SiC and 0.6904 J/g K for hexagonal SiC,[28] the SiC addition resulted in a slight increase of specific heat in the $Bi_{0.3}Sb_{1.7}Te_3$ + 0.4 vol% SiC composite. Please note that the measured C_p values are higher than the calculated values according to the rule of mixture, nevertheless the former values were used in this work for the computation of thermal conductivity. Then, the thermal conductivity is calculated from the measured thermal diffusivity, density and specific heat and the results are shown in Figure 6c.

Thermal conductivity can be expressed by the sum of lattice thermal conductivity (κ_L) and electronic thermal conductivity (κ_e), and κ_e can be estimated from Wiedemann-Franz's law as $\kappa_e = LT/R$, where T is the absolute temperature, R is the electrical resistivity and L is the Lorenz number. The classical value of the Lorentz number $L = 2.45 \times 10^{-8}$ V^2 K^{-2} and is valid for a degenerate electron gas. Here, $L = 2.0 \times 10^{-8}$ V^2 K^{-2} is used, which is used for a heavily doped semiconductor.[3,29] Therefore, κ_L is obtained using the equation $\kappa_L = \kappa - \kappa_e$. The temperature dependence of κ_L of both $Bi_{0.3}Sb_{1.7}Te_3$ and $Bi_{0.3}Sb_{1.7}Te_3$ + 0.4 vol% SiC are obtained and shown in Figure 6c with their thermal conductivity together. We can find that the electronic components κ_e of two samples make a great contribution to the total thermal conductivity, because of their lower electrical resistivity.

Finally, the temperature dependence of ZT values for $Bi_{0.3}Sb_{1.7}Te_3$ and $Bi_{0.3}Sb_{1.7}Te_3$ + 0.4 vol% SiC in temperature range from 300 to 500 K are given in Figure 6d. The maximum

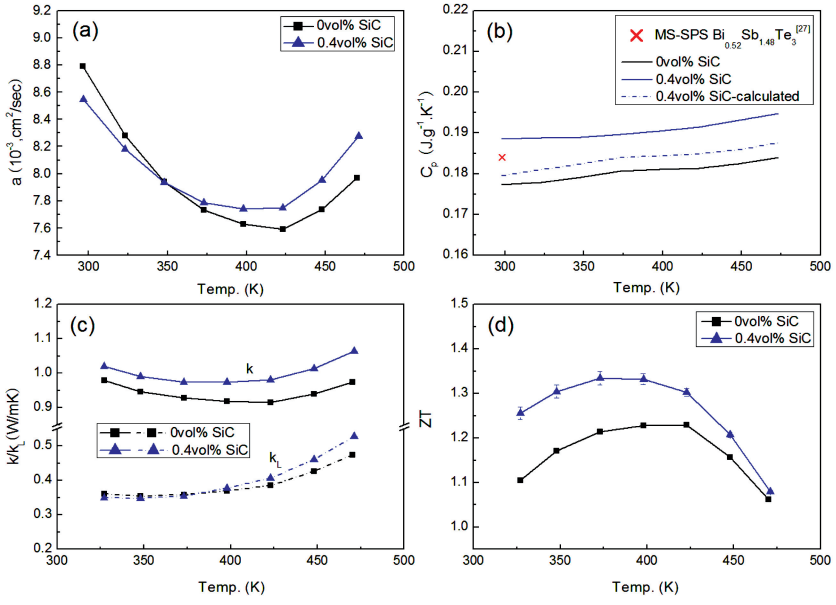

Figure 6. Temperature dependence of a) thermal diffusivity, b) measured heat capacity, c) thermal conductivity and lattice thermal conductivity, and d) ZT value for $Bi_{0.3}Sb_{1.7}Te_3$ and $Bi_{0.3}Sb_{1.7}Te_3$ + 0.4 vol% SiC samples.

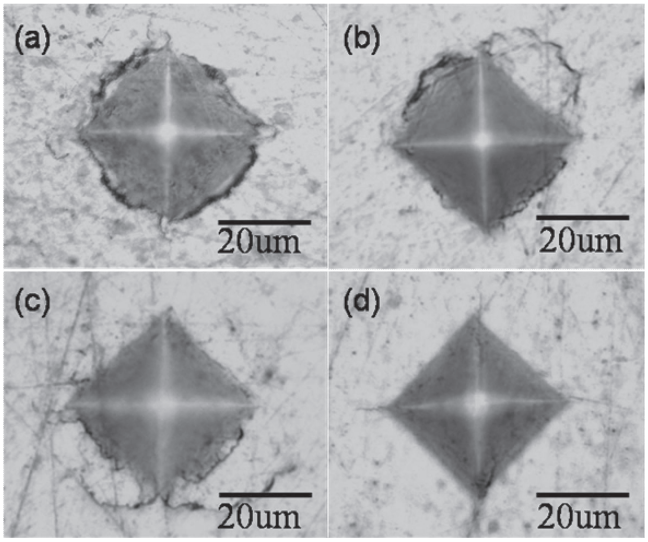

Figure 7. Microscopy images of indentation of $Bi_{0.3}Sb_{1.7}Te_3$ without and with different SiC content: a) 0 vol% SiC, b) 0.1 vol% SiC, c) 0.4 vol% SiC, and d) 0.6 vol% SiC.

ZT value of the present $Bi_{0.3}Sb_{1.7}Te_3$ sample without SiC is about 1.23 at 423 K, and $ZT > 1.2$ in the temperature rang from 373 to 423 K. The $Bi_{0.3}Sb_{1.7}Te_3$ + 0.4 vol% SiC composite gets a higher $ZT \approx 1.33$ at 373 K, because of the enhanced power factor and the unchanged thermal conductivity, and $ZT > 1.3$ in the temperature range from 373 to 423 K. It also should be mentioned that the present nanocomposites have better mechanical properties as an additional advantage, such as microhardness, which was tested by indentation method, and the microscopy images of indentation are shown in **Figure 7**. With SiC content increasing, the cracks in the samples decrease gradually, indicating that the resistance against cracking and fracture increases by the dispersion of SiC nanoparticles, since SiC possesses high Young's modulus and hardness, whose dispersion can lead to the improvement of fracture toughness (K_{IC}) in the composites.[12,13] The mechanical properties of thermoelectric materials have received attention recently, whose improvement is beneficial for improving the materials machinability and devices reliability.[14]

3. Conclusions

In summary, incorporating a small number of SiC nanoparticles into $Bi_{0.3}Sb_{1.7}Te_3$ alloys can enhance its thermoelectric performance to a high *ZT* value over 1.3 in a relatively wide temperature range, demonstrating that nanoinclusions in a thermoelectric compound matrix can both increase the Seebeck coefficient and electrical conductivity in addition to reducing phonon thermal conductivity if the nanoinclusions are well matched with the host material. Thermoelectric property improvement in the widely commercialized bismuth antimony telluride alloys is particularly meaningful, and the present nanocomposite approach may also be applicable to other thermoelectric materials. Nano-SiC-dispersed BiSbTe thermoelectric alloys should be more suitable for device fabrication for its better mechanical property and applications at elevated temperatures because of its improved thermoelectric performance at higher temperatures.

4. Experimental Section

Commercial elemental powders of Bi (99.99%, ≈75 μm), Sb (99.99%, ≈75 μm), Te (99.99%, ≈75 μm) and nano-SiC (99%, ≈100 nm) were used as starting materials. The mixtures of these powders were subjected to MA in a planetary ball mill using a hardened stainless steel vial and ball. The weight ratio of balls to powders was kept at about 20:1, and the mill vial was filled with Ar (99.99%) gas to prevent the powders from oxidation during the milling process. The milling was performed at 450 rpm for 3 h, and then the powders were consolidated by SPS at 673 K for 5 min under an axial pressure of 50 MPa, by which a series of $Bi_{0.3}Sb_{1.7}Te_3$ + *x* vol% SiC (*x* = 0, 0.1, 0.3, 0.4, 0.6) bulk materials were fabricated. It should be noted that the matrix composition was different from $Bi_{0.5}Sb_{1.5}Te_3$ for traditional zone-melting-made ingots, because our previous study revealed that the highest ZT value could be obtained in p-type $Bi_{0.3}Sb_{1.7}Te_3$ alloys prepared by a combined process of MA and SPS.[30]

The phase structure of all samples was examined by X-ray diffraction (XRD) using Cu Kα radiation (D/max-2500), and EPMA (JXA-8230, JEOL) was used to investigate the distribution of SiC nanoparticles in the $Bi_{0.3}Sb_{1.7}Te_3$ matrix. The microstructure was observed by SEM (JSM-6301) and field emission TEM (JEM-2010F). Specimens used for TEM were polished to about 30–40 μm and finally thinned to electron transparency using a precession ion-milling system at low angle (10–15°). HRTEM images of the pieces were recorded at 200 kV. The microhardness of $Bi_{0.3}Sb_{1.7}Te_3$ without and with different SiC content was carried out on a microhardness tester (HXD-1000), and the test load and dwell time was 0.5 N and 30 s, respectively. And the samples were prepared by fine grinding by hand

The carrier concentration and mobility were measured using the Hall measurement system (ResiTest 8400, Toyo, Japan). The Seebeck coefficient and electrical resistivity were measured using the Seebeck coefficient/electrical resistance measuring system (ZEM-2, Ulvac-Riko, Japan). The thermal conductivity (κ) was calculated using the equation $\kappa = \lambda C_p d$, where λ is the thermal diffusivity, C_p is the heat capacity, and *d* is bulk density of the sample. The thermal diffusivity was measured by the laser flash method (TC-9000, Ulvac-Riko, Japan) in vacuum in the temperature range from 300 to 500 K. The heat capacity was measured using a DSC (Q2000, TA, USA) and laser flash apparatus (LFA457, NETZSCH, German), and the bulk density was obtained by the Archimedes method.

Supporting Information

Supporting Information is available from the Wiley Online Library or from the author.

Acknowledgements

This work was supported by the National Nature Science Foundation (No. 51172121) and the National Basic Research Program of China (Grant No. 2013CB632503) as well as the national high technology research and development program (863 program, Grant No. 2012AA051104).

Received: January 14, 2013
Revised: February 20, 2013
Published online: April 10, 2013

[1] F. J. DiSalvo, *Science* **1999**, *285*, 703.
[2] J.-F. Li, W. S. Liu, L. D. Zhao, M. Zhou, *NPG Asia Mater.* **2010**, *2*, 152.
[3] M. S. Dresselhaus, G. Chen, M. Y. Tang, R. Yang, H. Lee, D. Z. Wang, Z. F. Ren, J. P. Fleurial, P. Gogna, *Adv. Mater.* **2007**, *19*, 1043.
[4] T. C. Harman, P. J. Taylor, M. P. Walsh, B. E. LaForge, *Science* **2002**, *297*, 2229.
[5] G. J. Snyder, E. S. Toberer, *Nat. Mater.* **2008**, *7*, 105.
[6] K. F. Hsu, S. Loo, F. Guo, W. Chen, J. S. Dyck, C. Uher, T. Hogan, E. K. Polychroniadis, M. G. Kanatzidis, *Science* **2004**, *303*, 818.
[7] M. Zhou, J.-F. Li, T. Kita, *J. Am. Chem. Soc.* **2008**, *130*, 4527.
[8] K. Biswas, J. Q. He, Q. C. Zhang, G. Y. Wang, C. Uher, V. P. Dravid, M. G. Kanatzidis, *Nat. Chem.* **2011**, *3*, 160.
[9] Y. C. Yan, A. J. Minnich, G. Chen, Z. F. Ren, *Adv. Funct. Mater.* **2010**, *20*, 357.
[10] X. Y. Zhao, X. Shi, L. D. Chen, W. Q. Zhang, S. Q. Bai, Y. Z. Pei, X. Y. Li, T. Goto, *Appl. Phys. Lett.* **2009**, *89*, 092121.
[11] V. Lankau, H. P. Martin, R. H. Weber, N. Oeschler, A. Michaelis, *J. Electron. Mater.* **2010**, *39*, 1809.
[12] J.-F. Li, J. Liu, *Phys. Status Solidi* **2006**, *203*, 3768.
[13] L. D. Zhao, B. P. Zhang, J.-F. Li, M. Zhou, W. S. Liu, J. Liu, *J. Alloys. Compd.* **2008**, *455*, 259.
[14] D. W. Liu, J.-F. Li, C. Chen, B. P. Zhang, L. L. Li, *J. Micromech. Microeng.* **2010**, *20*, 125031.
[15] L. D. Zhao, B. P. Zhang, J.-F. Li, H. L. Zhang, W. S. Liu, *Solid State Sci.* **2008**, *10*, 651.
[16] J. Jiang, L. D. Chen, S. Q. Bai, Q. Yao, Q. Wang, *Mater. Sci. Eng. B* **2005**, *117*, 334.
[17] Y. C. Lan, B. Poudel, Y. Ma, D. Z. Wang, M. S. Dresselhaus, G. Chen, Z. F. Ren, *Nano Lett.* **2009**, *9*, 1419.
[18] W. J. Xie, X. F. Tang, Y. G. Yan, Q. J Zhang, T. M. Tritt, *J. Appl. Phys.* **2009**, *105*, 113713.
[19] D. W. Liu, J.-F. Li, C. Chen, B. P. Zhang, *J. Electron. Mater.* **2011**, *40*, 992.
[20] E. S. Toberer, A. F. May, G. J. Snyder, *Chem. Mater.* **2010**, *22*, 624.
[21] C. J. Vineis, A. Shakouri, A. Majumdar, M. G. Kanatzidis, *Adv. Mater.* **2010**, *22*, 3970.
[22] Z. Xiong, X. H. Chen, X. Y. Zhao, S. Q. Bai, X. Y. Huang, L. D. Chen, *Solid State Sci.* **2009**, *11*, 1612.
[23] X. H. Yang, X. Y. Qin, *Appl. Phys. Lett.* **2010**, *97*, 192101.
[24] S. V. Faleev, F. Léonard, *Phys. Rev. B* **2008**, *77*, 214304.
[25] J. P. Heremans, V. Jovovic, E. S. Toberer, A. Saramat, K. Kurosaki, A. Charoenphakdee, S. Yamanaka, G. J. Snyder, *Science* **2008**, *321*, 554.
[26] J. R. Sootsman, D. Y. Chung, M. G. Kanatzidis, *Angew. Chem. Int. Ed.* **2009**, *48*, 8616.
[27] W. J. Xie, X. F. Tang, Y. G. Yan, Q. J. Zhang, T. M. Tritt, *Appl. Phys. Lett.* **2009**, *94*, 102111.
[28] M. Neuberger, *Mater. Res. Bull.* **1969**, *4*, S365.
[29] B. C. Sales, D. Mandrus, B. C. Chakoumakos, V. Keppens, J. R. Thompson, *Phys. Rev. B* **1997**, *56*, 15081.
[30] C. Chen, D. W. Liu, B. P. Zhang, J.-F. Li, *J. Electron. Mater.* **2011**, *40*, 942.